49th AIAA Aerospace Sciences Meeting including the New Horizons Forum and Aerospace Exposition
4 - 7 January 2011, Orlando, Florida
AIAA 2011-382

Active Flux Schemes

Timothy A. Eymann*
DoD HPCMP/CREATE Kestrel Team, Eglin AFB, FL 32542
Philip L. Roe†
Department of Aerospace Engineering, University of Michigan, Ann Arbor, MI, 48109

A class of active flux schemes is developed and employed to solve model problems for the linear advection equation and non-linear Burgers equation. The active flux schemes treat the edge values, and hence the fluxes, as independent variables, doubling the degrees of freedom available to describe the solution without enlarging the stencil. Schemes up to third order accurate are explored. Oscillations generated by the higher-order schemes are controlled through the use of a characteristic-based limiter that preserves true extrema in the solution without excessive clipping.

I. Introduction

We will investigate the possibilities of a relatively unexplored method for obtaining higher order accuracy in the numerical solution of conservation laws. All attempts at this must of course expand the degrees of freedom enjoyed by the algorithm. Here we explore both the possibility of extending the stencil in time rather than in space, and also the possibility of making the fluxes of a finite-volume scheme into active variables, that is to say, computing them from an evolution procedure rather than interpolating them from the cell-centered data.

In one dimension it turns out that these strategies are somewhat equivalent; an algorithm of one type can be rewritten as an algorithm of the other type. An advantage bestowed by this strategy is that the stencil becomes very compact in space, thereby minimizing the effects of mesh irregularity. Also, although the schemes can be made conservative, the flux variables need not be. This allows the use of non-conservative limiters, and introduces some flexibility.

In the context of conservation laws, there is in fact a family of such schemes. Members include the second author's upwind leapfrog scheme,[1] the CABARET scheme of Karabasov,[2] van Leer's Scheme V,[3] and the familiar first-order upwind scheme. Two other schemes belonging to this class are also discussed: a third order scheme using a compact stencil and a new optimum monotone scheme that outperforms the first-order upwind method.

II. Scheme basics

We begin by interpreting the data contained within a given cell as a quadratic function defined by Eq. (1), where $\bar{s_j}$ is the average slope for cell j, $\bar{c_j}$ is the average curvature, and x_j is the cell centroid coordinate. The slope and curvature are functions of the edge values and cell average $\bar{u_j}$

$$u(x) = \bar{u_j} + \bar{s_j}\left(\frac{x - x_j}{\Delta x}\right) + \bar{c_j}\left[\left(\frac{x - x_j}{\Delta x}\right)^2 - \frac{1}{12}\right] \tag{1}$$

This function is completely general. Its only notable property is that we recover the cell average $\bar{u}_j$ when $u(x)$ is integrated over each cell and multiplied by $1/\Delta x$. Expressions for the slope and curvature entirely determine the reconstruction and behavior of the scheme. For example, if one enforces the that the end points of the reconstruction are shared between cells and the reconstruction average is equal to the cell average, the resulting slope and curvature expressions are:

*Research Engineer, Ph.D. Candidate, Member AIAA
†Professor, Fellow AIAA

$$\begin{aligned} \bar{s}_j^n &= u_{j+\frac{1}{2}}^n - u_{j-\frac{1}{2}}^n \\ \bar{c}_j^n &= 3\left(u_{j+\frac{1}{2}}^n - 2\bar{u}_j^n + u_{j-\frac{1}{2}}^n\right) \end{aligned} \tag{2}$$

Equation (2) defines van Leer's Scheme V.[3] In the simple case of linear advection with $a > 0$, the Scheme V edge update and flux are:

$$u_{j+\frac{1}{2}}^{n+1} = u\left(x_{j+\frac{1}{2}} - \nu\Delta x\right) = (1-\nu)(1-3\nu)\,u_{j+\frac{1}{2}}^n + 6\nu(1-\nu)\,\bar{u}_j^n - \nu(2-3\nu)\,u_{j-\frac{1}{2}}^n \tag{3}$$

$$F_{j+\frac{1}{2}} = \frac{1}{\Delta t}\int_{x_{j+\frac{1}{2}}-\nu\Delta x}^{x_{j+\frac{1}{2}}} u(x)dx = (1-\nu)^2 f_{j-\frac{1}{2}}^n + \nu(3-2\nu)f_j^n - \nu(1-\nu)f_{j+\frac{1}{2}}^n \tag{4}$$

Scheme V is a classical finite volume scheme with a twist. The flux values at the cell interfaces are not just interpolated from nearby cell averages; they depend on previous flux values. They are therefore following evolution equations in which they appear as independent variables, thereby doubling the degrees of freedom available to describe the solution. For this reason, we refer to this class of schemes as *active flux* schemes.

The internal reconstructions of finite-volume schemes provide a strong physical and philosophical basis for the numerical simulation of fluids, but analysis of schemes is often easier in a finite-difference framework where it's more straightforward to apply techniques such as Fourier analysis and to apply concepts such as limiting and monotonicity. It turns out that all of the schemes in the class described above are, in a certain sense, equivalent to a three-level finite-difference scheme.

Since the centroid values and edge values are independent, we may represent any active flux scheme in terms of a 2×2 amplification matrix $\mathbf{G}$ such that

$$\begin{aligned} \begin{pmatrix} \bar{u}_j \\ u_{j+\frac{1}{2}} \end{pmatrix}^{n+1} &= \mathbf{G}\begin{pmatrix} \bar{u}_j \\ u_{j+\frac{1}{2}} \end{pmatrix}^{n} \\ \begin{pmatrix} \bar{u}_j \\ u_{j+\frac{1}{2}} \end{pmatrix}^{n+2} &= \mathbf{G}^2\begin{pmatrix} \bar{u}_j \\ u_{j+\frac{1}{2}} \end{pmatrix}^{n} \end{aligned} \tag{5}$$

Using the fact that every matrix satisfies its own characteristic equation, one can express the square of the amplification matrix as

$$\mathbf{G}^2 = \mathrm{tr}(\mathbf{G})\;\mathbf{G} - \det(\mathbf{G})\,\mathbf{I} \tag{6}$$

Substituting this expression into Eq. (5) and defining $\mathbf{q} = \left(\bar{u}_j, u_{j+\frac{1}{2}}\right)^{\mathsf{T}}$, we arrive at an expression for a three-level scheme in terms of the eigenvalues for a two-level scheme:

$$\begin{aligned} \mathbf{q}^{n+2} &= [\,\mathrm{tr}\,(\mathbf{G})\,\mathbf{G} - \det(\mathbf{G})\,\mathbf{I}\,]\,\mathbf{q}^n \\ &= \mathrm{tr}\,(\mathbf{G})\,\mathbf{q}^{n+1} - \det(\mathbf{G})\;\mathbf{q}^n \\ &= (\lambda_1+\lambda_2)\,\mathbf{q}^{n+1} - \lambda_1\lambda_2\;\mathbf{q}^n \end{aligned} \tag{7}$$

Equation (7) defines the relationship between two-level active flux schemes and three-level finite difference schemes. This allows us to design a three-level scheme with desirable dissipation or dispersion properties then express it as a two-level conservative scheme compatible with our finite-volume formulation.

III. Three-level family

The three-level stencil illustrated in Fig. 1 provides enough degrees of freedom to control a variety of numerical properties. The update at point 1 can be written as a combination of three residuals. Terms proportional to α in Eq. (8) comprise the residual evaluated over the triangle 2-4-5 (similarly for terms proportional to β, γ), while the terms not multiplied by any residual weights comprise the residual evaluated over triangle 1-2-3.

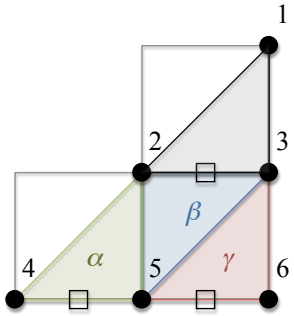

Figure 1. Three-level upwind stencil

$$\begin{aligned} u_1 \quad = \quad & [\nu - \alpha - \beta(1-\nu)]u_2 + [1 - \gamma - \nu(1+\nu)]u_3 + (\alpha\nu)u_6 + \\ & [\alpha(1-\nu) + \beta + \gamma\nu]u_7 + \gamma(1-\nu)u_8 \end{aligned} \tag{8}$$

The stencil above supports schemes up to fourth order accuracy; however, only schemes up to third-order were investigated for this preliminary work since they enjoy better dispersive properties than fourth order schemes. The residual weights α, β, and γ control the properties of the scheme. Table 1 lists the coefficient values that define notable schemes in the family.

Table 1. Residual weights

Scheme	$\mathcal{O}(\Delta x)$	α	β	γ
FUP	1	0	0	0
OPTM, $\nu < \frac{1}{2}$	1	0	$\frac{\nu}{1-\nu}$	0
OPTM, $\nu > \frac{1}{2}$	1	0	$\frac{1-\nu}{\nu}$	0
ULF	2	0	1	0
Chair	3	0	$\frac{3\nu}{1+\nu}$	$\frac{2\nu-1}{1+\nu}$
Scheme V	3	$-\nu^3$	$3\nu(1-\nu)$	$-(1-\nu)^3$

First order schemes can be defined by considering point 1 and two other points on the stencil. The simplest scheme is the familiar first order upwind (FUP) scheme of Courant, Isaacson, and Rees.[4] The optimum monotone scheme (OPTM) defined in the table is crafted to use only those points closest to the characteristic passing through point 1. The characteristic passes closest to points 3 and 5 when $\nu \leq \frac{1}{2}$. When $\nu > \frac{1}{2}$ the points closest to the characteristic are 2 and 5. We will return to this view of monotonicity and the concept of characteristic neighbors when developing our limiting strategy.

The most notable second order scheme in the family is the upwind leapfrog scheme (ULF), originally investigated by Iserles[5] and developed by the second author,[1] which has zero dissipation due to its stencil symmetry in space and time. However, the complete elimination of dissipation has been found to be insufficiently robust for practical use. We have found that the ULF scheme is greatly improved by the addition of extra points, which provide both third-order accuracy and some fourth order dissipation.

Much of this work focused on two of the third order schemes. Setting $\alpha = 0$ and using the remaining two parameters to eliminate both the leading diffusion and dispersion terms leads a third order scheme uniquely defined by points 1, 2, 3, 5, 6. We call the scheme the Chair Scheme since the stencil roughly takes this shape, as shown in Fig. 2. This is the only third order scheme that can be formulated over a single spatial interval and three time levels. The compactness of the scheme promises to make the it insensitive to mesh irregularities and to reduce message-passing requirements. However, it turns out to be stable only for $\nu \leq 1/2$.

The other third order scheme represented in the table is Scheme V. This scheme uses a larger stencil, which on the one hand may increase the sensitivity to mesh irregularity, but on the other hand extends the stability limit to a Courant number of $\nu = 1$. Additionally, the original derivation of Scheme V by van Leer is strongly physical, whereas we presently have only a formal derivation of the Chair Scheme.

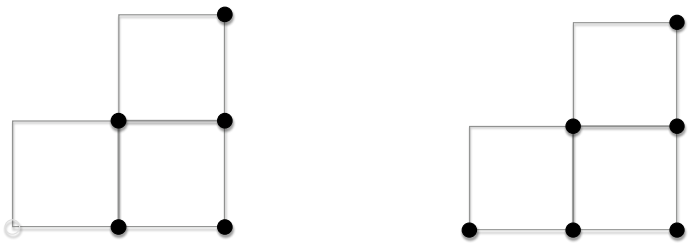

(a) Chair scheme (b) Scheme V

Figure 2. Third order stencils

A. Linear performance

We tested the OPTM scheme and the two third-order schemes on the linear advection equation with a suite of waveforms selected by Zaleszak[6] and others. The cases were run using a mesh of 132 equally-spaced cells as well as a mesh with randomized cell spacing. Figure 3 illustrates the increase in accuracy achieved by the OPTM scheme as a result of carefully selecting the stencil to respect the propagation of information. The OPTM is most accurate close to $\nu = \frac{1}{2}$, at which point it reproduces the exact solution. At the edges of the stability range ($\nu \approx 0$ and $\nu \approx 1$) the OPTM scheme produces solutions comparable to the FUP scheme.

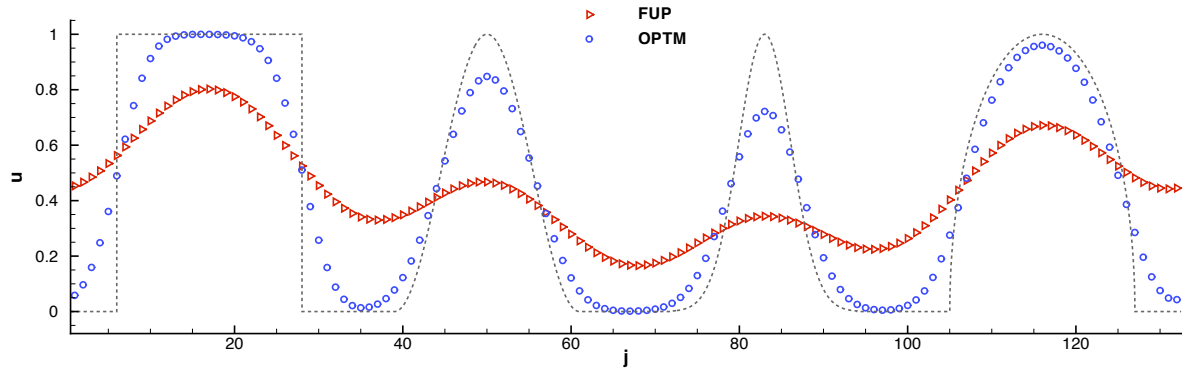

Figure 3. Monotone, first order schemes; $\nu = 0.44$

Surprisingly, there was very little difference between Scheme V and the Chair Scheme. This seems to be due to the fact that both schemes use a reconstruction within each cell based only information from that cell. Hence, the accuracy of each flux does not depend on any assumptions concerning the smoothness of the mesh. We therefore show results only for Scheme V, but compare them in Fig. 4 with results for a standard cubic-interpolating scheme due to Warming, Kutler, and Lomax[7] (WKL).

The more compact spatial stencil of Scheme V improves the accuracy compared to the cubic-interpolating scheme. On both the uniform and random meshes, Scheme V performs noticeably better on the narrow peak, and generally produces a solution closer to the exact solution. The active flux version, using universal weights, is also less expensive

because all interpolations are gone within a cell, as opposed to the WKL scheme, which uses interpolations that depend on the geometry of neighboring elements.

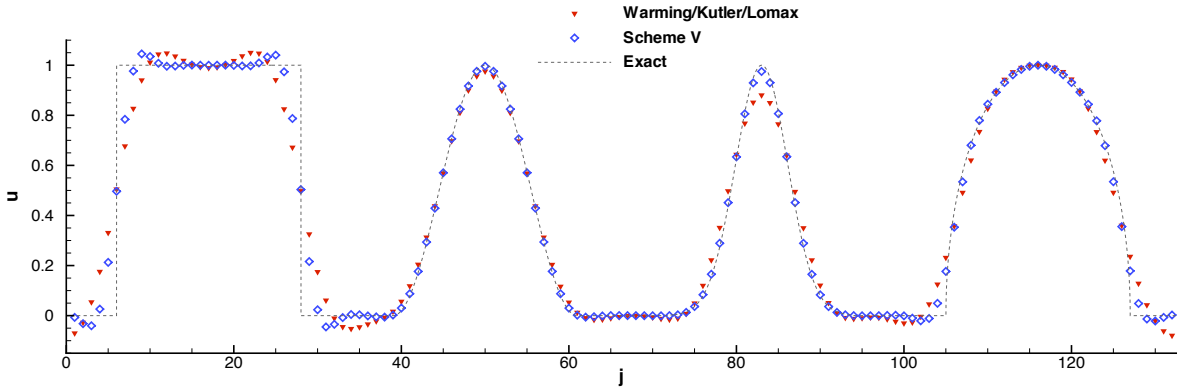

(a) Uniform mesh, $\nu = 0.44$

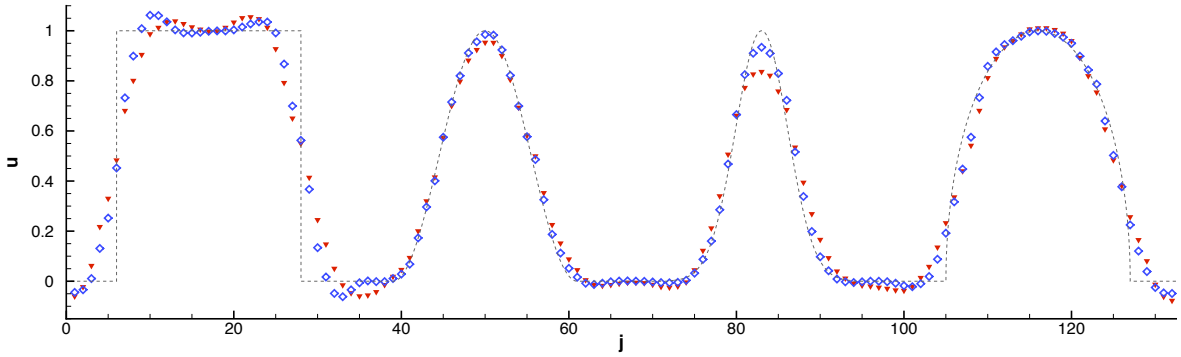

(b) Random mesh

Figure 4. Performance of third order schemes with compact and non-compact stencil

B. Limiting

None of the higher-order active flux schemes include any type of limiter, but of course any unlimited high-resolution scheme will generate oscillations that degrade the accuracy and robustness of the solver. Traditional limiting approaches often require the evaluation of neighboring data, expanding the effective stencil. Encouraged by the OPTM solutions, we employ a form of limiting that examines near neighbors in time. The strategy makes use of a "characteristic coordinate" concept illustrated in Fig. 5.

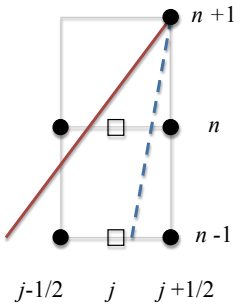

Figure 5. Characteristics for $\nu > \frac{1}{2}$ (solid) and $\nu < \frac{1}{2}$ (dotted)

Begin by finding those points in the stencil that are closest to the point $\left(j+\frac{1}{2}, n+1\right)$ in the characteristic coordinate $x-at$. Again, when $\nu < \frac{1}{2}$ these are the points at $\left(j+\frac{1}{2}, n\right)$ and $\left(j-\frac{1}{2}, n-1\right)$. When $\nu > \frac{1}{2}$, the characteristic neighbors are $\left(j-\frac{1}{2}, n\right)$ and $\left(j-\frac{1}{2}, n-1\right)$. If the edge update at $n+1$ is within the bounds of the appropriate set of characteristic neighbors, it is accepted, otherwise the value closest to this interval is used. By using the value at $\left(j-\frac{1}{2}, n-1\right)$, rather than the value at $\left(j-\frac{1}{2}, n\right)$ the limiter is made much milder in its operation. The following expression ensures that the node update does not exceed its characteristic neighbors:

$$u^* = \begin{cases} \min\left[u^{n+1}_{j+\frac{1}{2}}, \max\left(u^{n}_{j+\frac{1}{2}}, u^{n-1}_{j-\frac{1}{2}}\right)\right] & \text{if } \nu \leq \frac{1}{2} \\ \\ \min\left[u^{n+1}_{j+\frac{1}{2}}, \max\left(u^{n}_{j-\frac{1}{2}}, u^{n-1}_{j-\frac{1}{2}}\right)\right] & \text{if } \nu > \frac{1}{2} \end{cases} \tag{9}$$

Similar expressions keep the nodal update above the minimum of the characteristic neighbors. The flux at any interface where the node value has been limited is also modified. A new quadratic reconstruction of the internal cell state is created that shares the original cell average, but has an extrema passing through the limited value u^*. For positive wave speeds this leads to the following interface flux:

$$F_{j+\frac{1}{2}} = \frac{(1-2\nu)(1-\nu)f^*_{j+\frac{1}{2}} + \nu^2 f^n_j}{\nu^2 - 3\nu + 1} \tag{10}$$

Figure 6 shows the Scheme V solution with the characteristic-based limiter. Figure 7 overlays the solution generated with the unlimited solution and a Lax-Wendroff (LxW) solution with the superbee limiter. The results between the limited LxW scheme and Scheme V are comparable for the square wave, but for the Gaussian profile, the characteristic-based limiter does not suffer from either the excessive clipping or the "squaring" of the waveform.

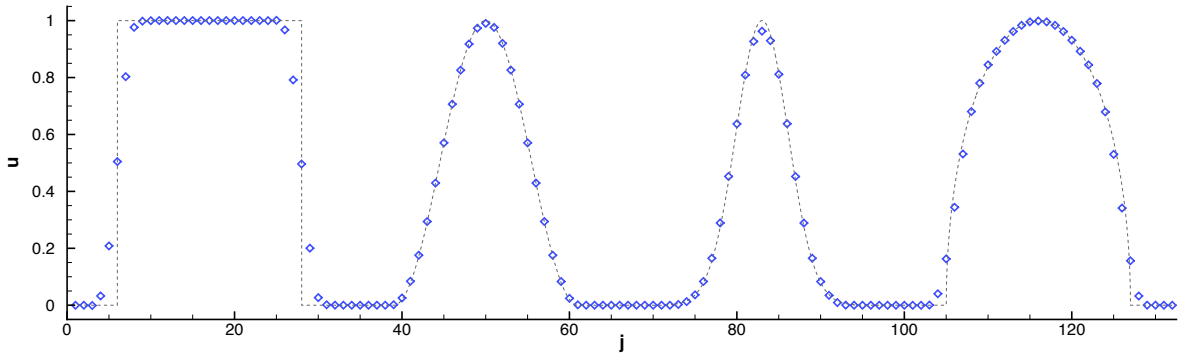

Figure 6. Limited Scheme V solution after one cycle; $\nu = 0.44$

Table 2. Peak values

(a) Random mesh

Wave	WKL	Scheme V
Square	1.055	1.062
Cosine	0.9532	0.9850
Gaussian	0.8365	0.9340
Ellipse	1.011	0.9994

(b) Uniform mesh

Wave	WKL	Scheme V	Scheme V (limited)
Square	1.050	1.040	1.001
Cosine	0.9756	0.9947	0.9903
Gaussian	0.8801	0.9745	0.9628
Ellipse	1.001	1.000	0.9987

Table 2 summarizes the peak values predicted by the third-order schemes on random and uniform meshes and includes limited results for the uniform mesh case. As illustrated by Fig. 6, Scheme V generally produces peak values closer to the expected value of 1.0. This limiting strategy ensures the TVD property for the nodal updates, but does not strictly enforce it upon the cell averages. Thus, this limiter tends to avoid the excessive clipping of legitimate extrema

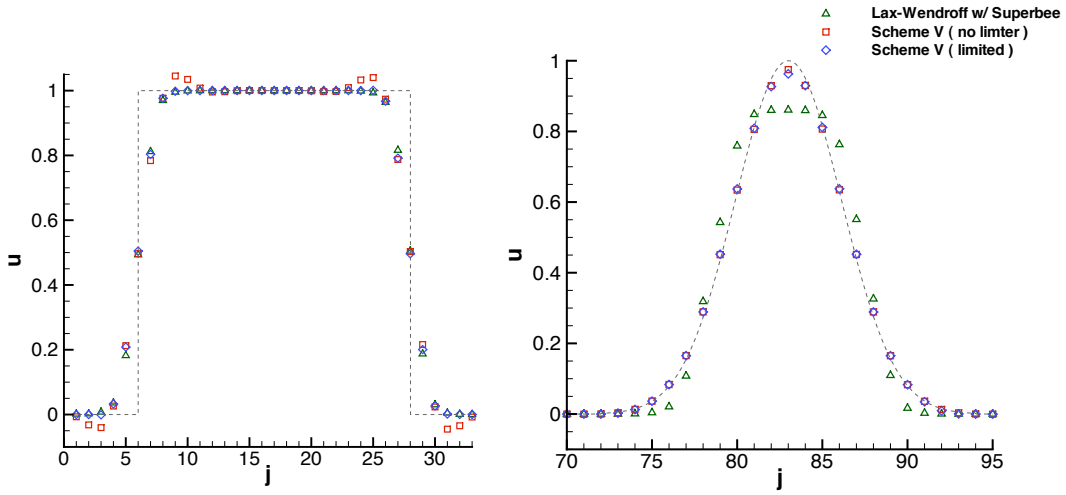

(a) Square wave (b) Gaussian

Figure 7. Limiter comparison after one cycle; $\nu = 0.44$

in the solution. The strategy is not, however conservative. In the next section, we reform the three-level schemes to be closer to a conventional finite-volume viewpoint, and at the same time restore conservation.

IV. Reformulation of the schemes

We seek to recover the three-level node update expression in Eq. (8) after two time steps. To achieve this goal, first define the flux at the cell interface as a third-order approximation to the time-averaged integral of $u(x)$.

$$F_{j+\frac{1}{2}} = \frac{1}{6}\left(f^n_{j+\frac{1}{2}} + 4f^{n+\frac{1}{2}}_{j+\frac{1}{2}} + f^{n+1}_{j+\frac{1}{2}}\right) \tag{11}$$

The analytical fluxes at time $n+1$ and $n+\frac{1}{2}$ are functions of the edge values. The update procedure used to calculate the new edge values from data at time n does not need to be conservative. A convenient method is to write the edge updates as generalized interpolations:

$$\begin{aligned} u^{n+\frac{1}{2}}_{j+\frac{1}{2}} &= \mu u^n_{j-\frac{1}{2}} + \phi \bar{u}^n_j + \psi u^n_{j+\frac{1}{2}} \\ u^{n+1}_{j+\frac{1}{2}} &= \xi u^n_{j-\frac{1}{2}} + \eta \bar{u}^n_j + \zeta u^n_{j+\frac{1}{2}} \end{aligned} \tag{12}$$

The approach bears some resemblance to the CABARET scheme[2] although that scheme can be interpreted as using a trapezoidal rule to determine the interface flux, fixing the global order of accuracy at second order. Our use of Simpson's Rule allows quadratic functions to be integrated exactly.

Next, the interpolation coefficients appearing in Eq. (12) must be related to the residual weights α, β, γ. As formulated, the system is underdetermined, consisting of five equations for six unknowns, resulting in one free parameter which we have taken to be ϕ. The rather inelegant algebra results in the following expressions for the interpolation coefficients of the two-level scheme in terms of the weights of the three-level scheme.

$$
\begin{aligned}
\xi &= -\frac{1}{6}\left[\alpha(6+\nu)+\beta(6-5\nu)+\nu(\gamma-5+4\phi)\right] \\
\eta &= 1+\alpha+\beta+\gamma \\
\zeta &= -\frac{1}{6}\left\{\gamma(6-\nu)-\nu[\alpha-5(1+\beta)+4\phi]\right\} \\
\mu &= \frac{9\alpha-\phi\{6(\alpha+\beta)-\nu[\alpha-5(1+\beta)+\gamma]\}-4\nu\phi^2}{6(1+\alpha+\beta+\gamma)} \\
\psi &= \frac{6(1+\beta+\gamma)-\phi[6+\gamma(6-\nu)+5\nu(1+\beta)]+4\nu\phi^2-\alpha(3-\nu\phi)}{6(1+\alpha+\beta+\gamma)}
\end{aligned}
\tag{13}
$$

When the flux function is known or reconstruction has already been defined, as with Scheme V, ϕ may be determined from the flux expression. In cases where the exact form of the reconstruction is unknown, ϕ should be selected to maintain desired characteristics (e.g. the reconstruction for the second order ULF scheme should reproduce linear data exactly). Table 3 repeats the residual weights and lists values of ϕ for selected second and third order schemes.

Table 3. Scheme definitions

Scheme	α	β	γ	ϕ
ULF	0	1	0	1
Chair	0	$\frac{3\nu}{1+\nu}$	$\frac{2\nu-1}{1+\nu}$	$\frac{3\nu}{1+\nu}$
Scheme V	$-\nu^3$	$3\nu(1-\nu)$	$-(1-\nu)^3$	$\frac{3}{2}\nu\,(2-\nu)$

The residual weights and parameter ϕ allow any scheme on the three-level stencil to be expressed as a two-level, finite-volume scheme with an active flux. The resulting flux expression may be compared to the integral of Eq. (1) to find the average slope and curvature as functions of the interpolation coefficients. For example, we can use the Chair Scheme definition above to develop expressions for the slope and curvature of the reconstruction:

$$
\bar{s}_j^n = \frac{6\nu(1-3\nu)\bar{u}_j^n + \left[4(1-2\nu)+6\nu^2(1+\nu)\right]u_{j+\frac{1}{2}}^n - 2\,(2-\nu)\left(1-3\nu^2\right)u_{j-\frac{1}{2}}^n}{(1+\nu)[1+3(1-2\nu)(1-\nu)]} \tag{14}
$$

$$
\bar{c}_j^n = \frac{6\,(2-\nu)\left(u_{j-\frac{1}{2}}^n - 2\bar{u}_j^n + u_{j+\frac{1}{2}}^n\right)}{(1+\nu)\,[1+3(1-2\nu)\,(1-\nu)]} \tag{15}
$$

The reconstruction, in turn, defines the appropriate two-level node update and flux:

$$
u_{j+\frac{1}{2}}^{n+1} = \frac{\nu(\nu-2)}{1+\nu}u_{j-\frac{1}{2}}^n + \frac{6\nu}{1+\nu}\bar{u}_j^n + \frac{(1-2\nu)\,(1-\nu)}{1+\nu}u_{j+\frac{1}{2}}^n \tag{16}
$$

$$
F_{j+\frac{1}{2}} = \frac{\nu(\nu-2)}{2(1+\nu)}f_{j-\frac{1}{2}}^n + \frac{3\nu}{1+\nu}f_j^n + \frac{2(1-\nu)-\nu^2}{2(1+\nu)}f_{j+\frac{1}{2}}^n \tag{17}
$$

In the schemes considered here, the fluxes are being updated according to a three-level finite-difference scheme, and the cell averages are then updated by using the fluxes to enforce conservation. The limiting procedure described in Section III-B can therefore be applied to the calculation of the fluxes without compromising conservation of the cell averages.

V. Burgers' equation

Given a successful scheme for linear advection, there are always many ways to devise nonlinear versions. We describe below just one version of Scheme V applied to Burgers' equation.

A. Fluctuations and signals

A convenient way to think about the numerical simulation of fluids is to consider "fluctuations" and "signals".[8] Define a fluctuation as something detected in the data indicating that it has not yet reached equilibrium, and a signal as an action performed on the data so as to bring it closer to equilibrium. Let a numerical fluctuation be defined as the difference between analytical fluxes at two points within the cell.

$$\delta_{j-\frac{1}{4}} = f_j - f_{j-\frac{1}{2}} \tag{18}$$

$$\delta_{j+\frac{1}{4}} = f_{j+\frac{1}{2}} - f_j \tag{19}$$

This fluctuation will generate a signal that propagates in the direction specified by the average wave speed over the interval. The magnitude of the signal depends on the scheme. Consider Scheme V. We may recast the flux expression for positive wave speeds as Eq. (20)

$$\begin{aligned} F_{j+\frac{1}{2}} &= f^n_{j+\frac{1}{2}} + \nu(1-\nu)\left(f^n_j - f^n_{j-\frac{1}{2}}\right) + \nu\left(\nu-2\right)\left(f^n_{j+\frac{1}{2}} - f^n_j\right) \\ &= f^n_{j+\frac{1}{2}} + \nu(1-\nu)\delta^n_{j-\frac{1}{4}} + \nu\left(\nu-2\right)\delta^n_{j+\frac{1}{4}} \end{aligned} \tag{20}$$

The node update may be represented in a similar fashion, where the fluctuation is now a difference in velocities.

$$u^{n+1}_{j+\frac{1}{2}} = u^n_{j+\frac{1}{2}} + \nu\left(3\nu-4\right)\left(u^n_{j+\frac{1}{2}} - \bar{u}^n_j\right) + \nu\left(2-3\nu\right)\left(\bar{u}^n_j - u^n_{j-\frac{1}{2}}\right) \tag{21}$$

One difference between solving the linear advection equation equation and Burgers' equation obviously lies in the analytical flux expressions for each (au for advection, $\frac{1}{2}u^2$ for Burgers). Another, more subtle, distinction is the definition of the Courant number ν. For non-linear equations, one must choose an appropriate wave speed to multiply the ratio $\Delta t/\Delta x$. In this work, we use the average speeds given by Eq. (22), allowing each half of the cell to have a different Courant number.

$$\begin{aligned} \bar{a}_{j-\frac{1}{4}} &= \frac{f_j - f_{j-\frac{1}{2}}}{\bar{u}_j - u_{j-\frac{1}{2}}} \\ \bar{a}_{j+\frac{1}{4}} &= \frac{f_{j+\frac{1}{2}} - f_j}{u_{j+\frac{1}{2}} - \bar{u}_j} \end{aligned} \tag{22}$$

When $\bar{a} > 0$, the signal is added to the right interface, and when $\bar{a} < 0$ the signal is subtracted from the left interface. The scaling coefficients for each signal are determined by its proximity to the interface with which it is associated. For the Scheme V fluxes, fluctuations closest to the interface are multiplied by a factor of $|\nu|\left(|\nu|-2\right)$ and those furthest from the interface are multiplied by $|\nu|\left(1-|\nu|\right)$. This approach may be generalized to the other schemes by writing the coefficients appearing in front of the fluctuations as functions of the interpolation coefficients from Eq. (12).

B. Non-linear performance

The scheme was tested on two cases; a Gaussian pulse and a centered expansion wave. The Gaussian pulse starts with the following initial data:

$$u_0(x) = \frac{1}{20} + \frac{19}{20}e^{-50\left(x-\frac{1}{2}\right)^2} \tag{23}$$

Straightforward analysis shows that a shock forms at time $t_s = 0.174$ and position $x_s = 0.709$. The initial speed of the shock is $u_s = 0.63$, but it slows and weakens as it interacts with the expansion. Our implementation of Scheme V performed well up to the time shock formation, but after that, the scheme began producing excessive overshoots in the conserved variables. The characteristic-based limiter did control the extrema in the edge values, but had little effect on the cell averages.

The solution of the Gaussian pulse indicates that our initial choices for the non-linear implementation of the active flux schemes may be improved upon. As an intermediate step, we have chosen to use the procedure outlined above in smooth regions of the flow and employ an exact Riemann solution at interfaces where neighboring characteristics intersect. The characteristic speed was estimated using the average wave speed defined in Eq. (22), and if the time of intersection is sufficiently close to the current time, the interface state from the Riemann solution is used to calculate the flux. However, by using only the Riemann solution as the basis for the flux, we are effectively introducing excessive dissipation and dropping to first order accuracy. For this reason, we attempt to resort to it as little as possible. Figure 8 shows the solution at the time of shock formation and the same simulation a period of time after the shock first forms, illustrating the difference between results with and without Riemann solves.

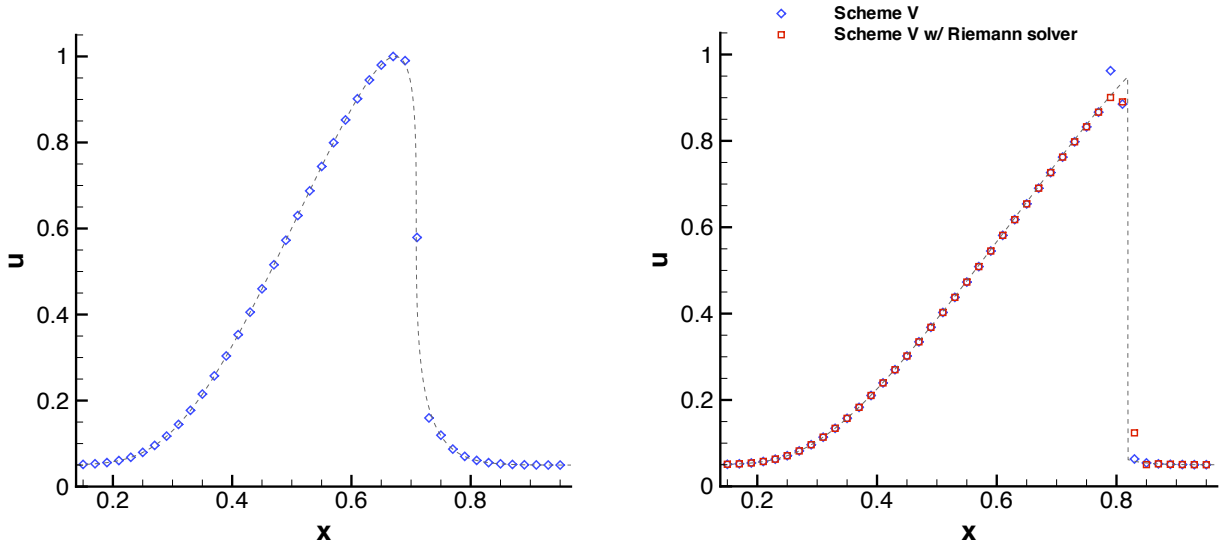

(a) $t = 0.174$ (b) $t = 0.375$

Figure 8. Solution of Gaussian pulse at shock formation (left) and post shock formation (right). Exact solution shown with dotted line.

We also tested Scheme V on a expansion containing a sonic point, created by specifying the initial data given in Eq. (24).

$$u_0(x) = \begin{cases} -\frac{1}{2} & \text{if } x \leq \frac{1}{2} \\ 1 & \text{if } x > \frac{1}{2} \end{cases} \tag{24}$$

A sonic expansion presents an additional challenge for schemes. The difficulty lies in crafting a flux that spreads the wave at the sonic point rather than preserving it as a non-physical expansion shock. Unfortunately, our initial results revealed that our approach was doing the latter. The scheme outlined in the previous section sends no signals to an interface surrounded by diverging characteristics, hence there is no mechanism to break up an expansion wave. We modified the scheme to also apply the Riemann solver in these regions. The modified scheme produces acceptable results, but as shown in Fig. 9, the Riemann-derived fluxes cause the cell averages to deviate from the exact solution near the sonic point. To further improve the results, the sonic flux formula developed by the second author[9] was implemented and applied whenever a sonic point was detected. In cells where $\bar{a}_{j-\frac{1}{4}} < 0 < \bar{a}_{j+\frac{1}{4}}$, the sonic flux defined in Eq. (25) was used at both the left and right interface of the cell. This approach produced a smooth solution throughout the expansion. While the sonic flux produced the best results for the particular case of an expansion lying within a cell, more investigation and development may be required to ensure the flux function works for all cases.

$$F_{j+\frac{1}{2}} = \frac{1}{2}\left[F_{j+\frac{3}{2}} + F_{j-\frac{1}{2}} - \frac{(u_{j+1} - u_j)^2}{1 + (u_{j+1} - u_j)\,\frac{\Delta t}{\Delta x}}\right] \tag{25}$$

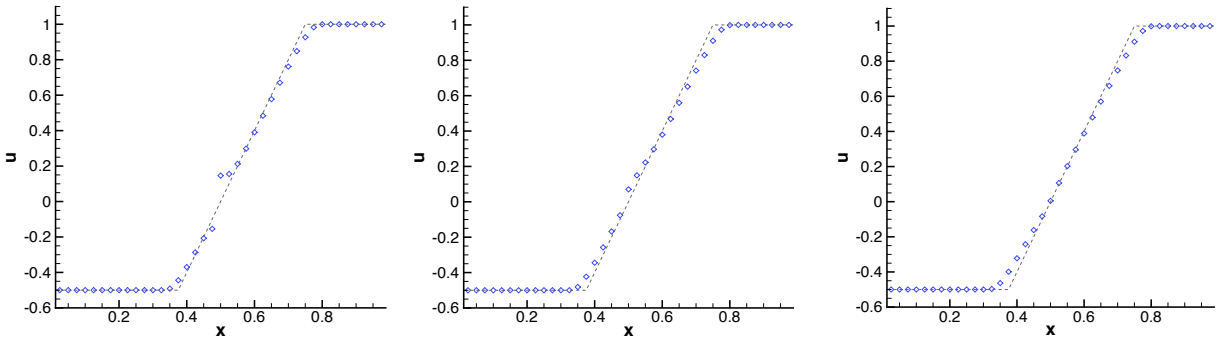

(a) No entropy-fix (b) Riemann solution (c) Sonic flux

Figure 9. Scheme V expansion with sonic point. Exact solution shown with dotted line.

VI. Summary and extensions

Active flux schemes, when combined with a characteristic-based limiter, have shown great potential for the solution of hyperbolic conservation laws. The scheme, as presented, performs well on linear advection problems. Non-linear solutions currently require the use of a Riemann solver, but the schemes' flexibility and demonstrated accuracy in smooth regions give us confidence that alternate approaches will reduce the need for such a blunt tool. The solutions presented in this paper merely represent our first attempt at solving non-linear problems with the schemes.

It should be noted that highly-parallel CFD simulations using unstructured meshes are becoming the de-facto approach for many aerospace applications. Traditional methods of increasing the order of accuracy of finite-volume schemes often involve expanding the computational stencil, requiring additional computations (interpolations) on unstructured meshes and degrading the parallel efficiency. Other higher-order methods that maintain a compact stencil, such as discontinuous Galerkin or spectral methods, do so at an increased computational expense. The extremely compact stencil and relatively low cost of the active flux schemes make them an attractive candidate for high-performance simulations using irregular meshes.

These ideas extend very naturally to higher dimensions. Six degrees of freedom are required for third order accuracy in 2-D. A seventh may be added as a symmetrical "bubble function" to ensure conservation. A natural location for the conserved variable is at the triangle centroid, leaving six locations at which to store solution data that does not need to be conserved (i.e. fluxes). An obvious choice is to store flux data at the three cell vertices and three edge midpoints. For 3-D tetrahedra, the vertices and edges also provide the correct degrees of freedom. In either the two or three-dimensional case, once a location for the variables is determined, all the 1-D concepts of carefully conserving centroid data while updating flux data using appropriate upwinding may be directly applied. Exploring which higher-dimension approach is the most effective will be a major portion of the next phase of this work.

References

[1]Roe, P., "Linear Bicharacteristic Schemes Without Dissipation," *SIAM Journal of Scientific Computing*, Vol. 19, No. 5, 1998, pp. 1405–1427.

[2]Karabasov, S. and Goloviznin, V., "Compact Accurately Boundary-Adjusting high-REsolution Technique for fluid dynamics," *Journal of Computational Physics*, Vol. 228, 2009, pp. 7426–7451.

[3]van Leer, B., "Towards the Ultimate Conservative Difference Scheme. IV. A New Approach to Numerical Convection," *Journal of Computational Physics*, Vol. 23, No. 3, 1977, pp. 276–299.

[4]Courant, R., Isaacson, E., and Rees, M., "On the solution of nonlinear hyperbolic differential equations by finite differences," *Comm. Pure Appl. Math*, Vol. 5, No. 3, 1952, pp. 243–255.

[5]Iserles, A., "Generalized Leapfrog Methods," *IMA Journal of Numerical Analysis*, Vol. 6, 1986, pp. 381–392.

[6]Zalesak, S. T., "Fully Multidimensional Flux-Corrected Transport Algorithms for Fluids," *Journal of Computational Physics*, Vol. 31, No. 3, 1979, pp. 335–362.

[7]Warming, R., Kutler, P., and Lomax, H., "Second- and Third-Order Noncentered Differnce Schemes for Nonlinear Hyperbolic Equations," *AIAA Journal*, Vol. 11, No. 2, 1973, pp. 189–196.

[8]Roe, P. L., "Fluctuations and Signals - A Framework for Numerical Evolution Problems," *Numerical Methods for Fluid Dynamics*, 1982, pp. 219–257.

[9]Roe, P., "Sonic Flux Formulae," *SIAM Journal on Scientific and Statistical Computing*, Vol. 13, No. 2, 1992, pp. 611–630.